American Mineralogist, Volume 93, pages 573–583, 2008

Crystal structures of synthetic melanotekite ($Pb_2Fe_2Si_2O_9$), kentrolite ($Pb_2Mn_2Si_2O_9$), and the aluminum analogue ($Pb_2Al_2Si_2O_9$)

G. Dörsam,[1,*] A. Liebscher,[1] B. Wunder,[2] and G. Franz[1]

[1]Fachgebiet Mineralogie und Petrologie, Technischen Universität Berlin Ackerstr. 76, D-13355 Berlin, Germany
[2]GeoForschungsZentrum Potsdam, Department 4, Telegrafenberg, D-14473 Potsdam, Germany

Abstract

Synthetic crystals of melanotekite and kentrolite were obtained at 850 °C from melt. The aluminum analogue of kentrolite $Pb_2Al_2Si_2O_9$ was hydrothermally synthesized at 2 GPa, 650 °C together with zoisite-(Pb) and margarite-(Pb). Synthesis products were characterized by single-crystal diffraction studies and microprobe analysis.

The aluminum analogue $Pb_2Al_2Si_2O_9$ was observed in space group *Pbcn* with lattice parameters $a = 6.8981(7)$ Å, $b = 10.6906(15)$ Å, $c = 9.7413(10)$ Å, and $V = 718.37$ Å^3. Fourier mappings show no irregularities of the Pb site.

Melanotekite with lattice parameters $a = 6.9786(6)$ Å, $b = 11.0170(11)$ Å, $c = 10.0895(9)$ Å, and $V = 775.71(17)$ Å^3 in space group *Pbcn* show a slightly deformed Pb-position in Fourier mappings.

Kentrolite was observed in space group $P2_122_1$ with pseudo-symmetry to *Pbcn* with lattice parameters $a = 7.0103(5)$ Å, $b = 11.0729$ (7) Å, $c = 9.9642(7)$ Å, and $V = 773.47(11)$ Å^3. Fourier mappings of the kentrolite structure show that two different split Pb sites exist, which causes lower symmetry. The unit-cell volume of different members of the kentrolite group is a linear function of trivalent ionic radii in sixfold coordination for the elements Al, Ga, In, and also for Fe and Mn in high spin mode.

The structure of $Pb_2M_2Si_2O_9$ ($M = Al^{3+}$, Fe^{3+}, Mn^{3+}) is built on isolated M-octahedra chains parallel **c**, M-octahedra sharing alternately *trans* and *skew* edges. Each Si_2O_7-group is linked with their vertices to three octahedra chains. Their Si-O-Si bond angles depend on the size of M-octahedra and are 129.84° in $Pb_2Al_2Si_2O_9$, 131.08° in $Pb_2Fe_2Si_2O_9$, 128.34° and 130.33° in $Pb_2Mn_2Si_2O_9$.

Keywords: Kentrolite, melanotekite, $Pb_2Al_2Si_2O_9$, $Pb_2Fe_2Si_2O_9$, $Pb_2Mn_2Si_2O_9$, crystal-structure, X-ray-diffraction, EMP-analysis

Introduction

Kentrolite ($Pb_2Mn_2Si_2O_9$) is a rare mineral and occurs mainly in Mn- and Pb-leading skarn ore deposits. It was found, i.e., in Tsumeb, Otjikoto (Namibia) and in Långban, Filipstad, Värmland, (Sweden).

Kentrolite is an orthorhombic sorosilicate with Si_2O_7-groups with Si-O-Si-dimers aligned to [100]. The Si_2O_7-groups are associated with edge-shared ($Mn^{3+}O_6$) octahedra, which build an infinite octahedral chain parallel [001]. These octahedra are alternately *trans* and *skew* with respect to adjacent octahedra (Moore et al. 1991; Barbier and Lévy 1998), see Figure 1.

The linkage of octahedra chains in the kentrolite group can be related to other known crystal structures, i.e., the borax structure $[Na(H_2O)_4]_2[B_4O_5(OH)_4]$, with sodium as central atom in the octahedron. The octahedra chains in borax are bonded with hydrogen and B_2O_7-BO_3 groups. The octahedra chain of kentrolite also closely resembles the infinite $[MnO_4]$ chain of the synthetic phase CMS-X1 $Ca_3Mn_2O_2(Si_4O_{12})$, which was found next to piemontite (Anastasiou and Langer 1977).

The complete $Pb_2(Mn,Fe)_2Si_2O_9$ solid-solution series was studied by Ito and Frondel (1966). The end-members with Cr, Ga, Sc, and In were synthesized by Ito and Frondel (1968) and Ito (1968).

The first crystal-structure model of natural kentrolite ($Pb_2Mn_2Si_2O_9$) is given in space group $C222_1$ based on Weissenberg photographs from Gabrielson (1961). Later, Ito and Frondel (1966) synthesized solid-solution series between the Mn and Fe end-member, $Pb_2Fe_2Si_2O_9$, named melanotekite. Lattice parameter refinement within the solid solution showed a linear relation with X_{Fe} based on powder-XRD data.

Gabelica-Robert and Tarte (1979) subsequently synthesized the known kentrolite structures and additional Ge-analogues and also structures with double substitution $2M^{3+} \rightarrow M^{2+} + M^{4+}$ with M^{2+} (Mg, Co, Ni, Cu) and M^{4+} (Ti, Sn). They found no common linear behavior of lattice parameters of these kentrolite end-members based on the ionic radii (Shannon 1976) of the transition metals of the fourth period. In particular, kentrolite structures with Mn^{3+} and Cu^{2+} differ significantly in lattice parameters as expected from ionic radii. From IR and Raman spectroscopy, these authors suggested a lower symmetric space group than $C222_1$, however without providing a structure solution.

* E-mail: guido.doersam@web.de

Single-crystal diffraction study of a natural melanotekite-kentrolite crystal with X_{Mn} = 0.68 was described by Moore et al. (1991) in space group *Pbcn*. This structure model is well described by Moore et al. (1991) and differs strongly from the previous one and is most likely the correct structure model for the kentrolite group because interatomic distances and angles are more believable. However, the authors noticed that the $6s^2$ Pb^{2+} lone-pair cations are split asymmetrically in two positions with site occupation factors (SOF) Pb1 SOF = 0.73 and Pb2 SOF = 0.27, but could not explain why. Werner and Müller-Buschbaum (1997) synthesized $Pb_2In_2Si_2O_9$ in space group $Pna2_1$, what can be expressed as $P2_1cn$, a non-centrosymmetric subgroup of *Pbcn*. This structure contains isotypic units of Si_2O_7-groups and the same linkage with M-octahedra chains as the model of Moore et al. (1991) but no split of the Pb site and lack of an inversion center.

Barbier and Lévy (1998) synthesized the germanate analogue of melanotekite with the formula $Pb_2(Fe_{1.78},Mg_{0.11},Ge_{0.11})Ge_2O_9$ in space group *Pbcn* and showed further that the structure is relatively flexible for solid solutions with Mg and Ge on the M sites (X_{Fe} = 0.89), and for Ge on the T sites. They observed also a split of the Pb-site with Pb1 SOF = 0.91 and Pb2 SOF = 0.09. In principle all these works show that the Pb site complicates space group determination, structure solution and refinement, whereas only small changes occur in T_2O_7-group and the infinite $(M^{3+}O_4)$-chains.

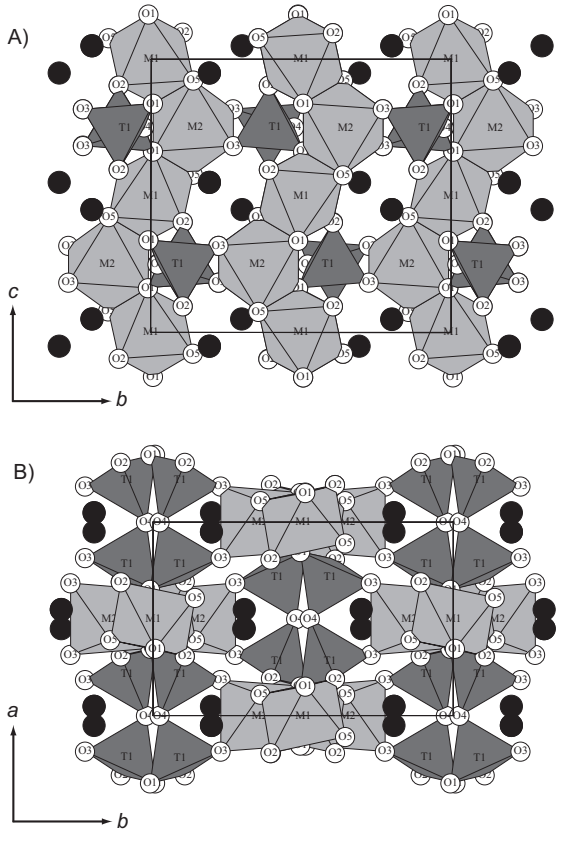

FIGURE 1. Crystal structure of $Pb_2Al_2Si_2O_9$ in space group *Pbcn*, (**a**) projection from **a** on the **b-c** plane, and (**b**) from **c** on the **a-b** plane.

In general, the problem with the split Pb-site is observed in several other Pb-bearing phases, i.e., in Pb-hollandite, a split Pb site was found (Downs et al. 1995); in feldspar-(Pb), the split Pb site was observed as an effect of thermal treatment (Tribaudino et al. 1998). In phoenicochroite [$PbO(CrO_4)$], no splitting in Pb site was observed however, lead atoms build (Pb_2O)-cluster chains with relatively short Pb-Pb distances of 3.56 Å (Morita and Toda 1984). Krivovichev and Burns (2001, 2002 and references therein) found (Pb_4O)-clusters in lead oxide chlorides. In contrast to strontium and barium, lead in the oxidation state Pb^{2+} can build a $6s^2$ lone pair and is able to compensate for strain within the structure. Therefore Pb^{2+}-cations must not necessarily be placed in a closed coordination polyhedron [see crystal structure of damaraite (Krivovichev and Burns 2001), with 6 different coordinated lead sites].

All these observations show clearly that lead atoms have a different chemical character than other isovalent elements with similar size. Here, we report first on the crystal structure of synthetic $Pb_2Al_2Si_2O_9$. Then, we give crystal structures of kentrolite ($P2_122_1$) and melanotekite (*Pbcn*) based on single-crystal diffraction studies, and finally, we discuss structural differences within the kentrolite group.

EXPERIMENTAL SETUP AND MICROPROBE ANALYSES

A list of synthesis conditions for the kentrolite isotypes with Al, Ga, In, and the transition metals from the literature is summarized in Table 1. All phases were synthesized between 1 atm and 2 GPa and 450 and 4053 °C. CIF[1] is available via the web.

High-pressure synthesis of $Pb_2Al_2Si_2O_9$

At 1 atm pressure, the phase diagram of the ternary system PbO-Al_2O_3-SiO_2 (Chen et al. 2001) does not indicate the stability nor the existence of $Pb_2Al_2Si_2O_9$;

[1] Deposit item AM-08-016, CIF. Deposit items are available two ways: For a paper copy contact the Business Office of the Mineralogical Society of America (see inside front cover of recent issue) for price information. For an electronic copy visit the MSA web site at http://www.minsocam.org, go to the American Mineralogist Contents, find the table of contents for the specific volume/issue wanted, and then click on the deposit link there.

TABLE 1. Synthesis conditions for kentrolite $Pb_2M_2Si_2O_9$ isotypes

M^{3+} [VI]	*T* (°C)	*P* (GPa)	Crystal size and structural info	Source
Al	650	2*	Single crystal (150 µm)	this study
Fe	850	Air†	Single crystal (60 µm)	this study
Mn	850	Air†	Single crystal (200 µm)	this study
Ga	450	0.2*	Powder	Ito and Frondel (1968b)
Ga	850–900	Air	No crystals	Gabelica-Robert and Tarte (1979)
In	<1050	Air†	Single crystal	Werner and Müller-Buschbaum (1997)
In	900	Air	Powder	Ito (1968a), Gabelica-Robert and Tarte (1979)
In	500	0.2*	Powder	Ito (1968a)
Sc	450	0.2*	Powder	Ito and Frondel (1968b)
Sc	900	Air	Powder	Gabelica-Robert and Tarte (1979)
Cr	450	0.2*	Powder	Ito and Frondel (1968b)
Cr	875	Air	Powder	Gabelica-Robert and Tarte (1979)
Fe	480	0.2*	(300 µm)	Ito and Frondel (1966)
Fe	875	Air	Powder	Gabelica-Robert and Tarte (1979)
Mn	480	0.2*	(300 µm)	Ito and Frondel (1966)
Mn	900	Air	Powder	Gabelica-Robert and Tarte (1979)

* Hydrothermal.
† Crystallization from melt.

however, two other phases, $Pb_4Al_4Si_5O_{20}$ and $Pb_4Al_4Si_3O_{16}$, are shown that have excess or lack of SiO_2 compared to kentrolite-(Al). We obtained kentrolite-(Al) from high-pressure experiments at 2.0 GPa and 650 °C. In our experiment, which was originally aimed to synthesize zoisite-(Pb), a mixture of 7.51 mg α-SiO_2 (99.99%), 19.509 mg $PbAl_2O_4$ (synthetic, from γ-Al_2O_3 and PbO by heating at 800 °C in a corundum-crucible), and 4.464 mg PbO (99.99%) was ground and homogenized in acetone. Thirty-five microliters of distilled H_2O were injected in a Pt capsule (12 mm long and 3 mm in diameter), 25 mg of the mixture were added and the capsule sealed. The capsule was placed in a NaCl-graphite assembly. Pressure was set in an unloaded piston cylinder press to 2.0(1) GPa and temperature kept constant at 650(5) °C for 6 days, controlled by a Ni-CrNi thermocouple. Details for the piston-cylinder experiment are given by Wunder and Melzer (2002).

High-temperature synthesis of $Pb_2Mn_2Si_2O_9$ and $Pb_2Fe_2Si_2O_9$

Suitable crystals of end-members $Pb_2Mn_2Si_2O_9$ and $Pb_2Fe_2Si_2O_9$ were obtained by crystallization of PbO-enriched melt. We mixed the oxides PbO, Fe_2O_3, and SiO_2 in stoichiometric amounts with excess of PbO to compensate its volatilization and placed the melanotekite mixtures on platinum plates (for kentrolite we used MnO_2 instead of Fe_2O_3). Mixtures were heated up to 1100 °C for complete melting. Temperature was reduced to 850(10) °C within an hour and held for two days. After that, samples were quenched in air.

Microscopic observations

In contrast to melanotekite and kentrolite, which have strong orange-red and red colors, the Al-analogue appears colorless in transmitted light. Electron microprobe analyses (EMP) were performed on polished and carbon coated samples with a Cameca SX 50 microprobe using wavelength dispersive spectrometry (WDS) and the PAP correction program (Pouchou and Pichoir 1984). Acceleration voltage was 10 kV, beam current 15 to 20 nA, and beam diameter was 1 µm. The following wavelengths and analyzator crystals were used: Si*K*β (TAP), Al*K*α(TAP), Mn*K*α (PET), Fe*K*α (LIF), and Pb*M*α (PET) . Standard for Si and Al was synthetic kyanite; for Fe and Mn we used pure metals. For Pb we started to use PbO and Pb-metal as standards. However, this resulted in large errors and implausible oxide sums. Therefore, we used the synthetitic kentrolite-(Al) ($Pb_2Al_2Si_2O_9$) itself as standard for Pb, assuming an ideal stoichiometry. The method was checked by analyzing other synthetic Pb-silicates margarite-(Pb) $PbAl_4Si_2O_{10}(OH)_2$, zoisite-(Pb) $Pb_2Al_3Si_3O_{12}(OH)$, which occurred together with kentrolite in this high-pressure experiment and lawsonite-(Pb) $PbAl_2[(OH)_2/Si_2O_7]\cdot H_2O$ as well as plumbotsumite $[Pb_5Si_4O_8(OH)_{10}]$ from other experiments synthesized at 4 GPa and 600 °C (Table 2). The results indicate that Pb is still slightly higher than in the ideal formula, but satisfying for the purpose of our study because the results show that the Pb-position in the structure is completely occupied.

Synthetic kentrolite was found to be euhedral with small braunite (Mn_7SiO_{12}) inclusions in a matrix with lead-orthosilicate (Pb_2SiO_4) composition (Fig. 2). In contrast to kentrolite-(Al) and kentrolite, the crystal size of melanotekite was small and some crystals contain fine inclusions of hematite (Fe_2O_3).

Results

$Pb_2Al_2Si_2O_9$

Single, transparent, clear, idiomorphic, prismatic crystals, up to 150 µm length were obtained and used for single-crystal diffraction studies and microprobe analysis. Experimental details of the data collection for the structure determination are summarized in Table 3. The λ/2-effect caused weak additional intensities and first we assumed a larger cell with doubled lattice parameter. But the weak intensities were only present close to the center (000) and disappear with increasing n. In reciprocal space, we choose the larger cell, and sampled over all matching intensities of the orthorhombic cell with the parameters a = 6.8981(7) Å, b = 10.6906(15) Å, and c = 9.7413(10) Å. Using this approach, weak intensities at the half of the reciprocal lattice were so rejected. But still some weak intensities caused by λ/2-effect, remain on the chosen lattice. The data were not further corrected for λ/2-effect.

To account for the strong absorption coefficient of Pb, we corrected the data with a spherical absorption model. Structure solution was done with direct methods, using the program SIR92 (Altomare et al. 1992). Statistical tests on the |E| values indicated strongly the existence of an inversion center. Space group determination suggested *Pbcn* with the best fit. Intensities, which do not fit with *Pbcn* and seem to be caused by λ/2-effect (Table 4), were not used in our final structure model. Structure solutions and refinements (SHELXL-97 program; Sheldrick 1993) in possible subgroups of *Pbcn*, $P112_1/n$, $P2_1/b11$, $P2_1cn$, $Pb2n$, and $P\bar{1}$ were all done, but all of them were not using these intensities either and delivered negative U_{iso} values. With respect to the work of Werner and Müller-Buschbaum (1997), we tried structure solution in space group $P2_1cn$, which converged with a R_1 of 13%. Further structure refinement with weighting parameters, extinction, and anisotropic displacement factors, and a twinning matrix ($\bar{1}$ 0 0) (0 $\bar{1}$ 0) (0 0 1) suggested from the Platon program

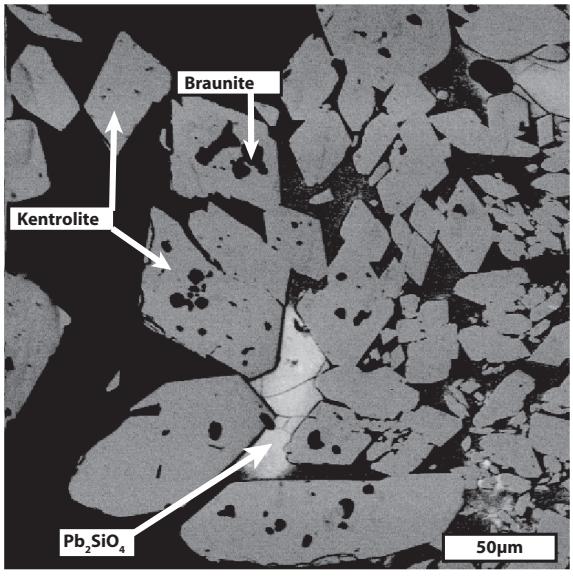

Figure 2. BSE-image shows euhedral kentrolite crystals with small braunite inclusions in a matrix with Pb_2SiO_4 composition.

Table 2. Electron microprobe analyses of Pb-bearing phases (wt%)

Phases	Points	Al_2O_3	SiO_2	PbO	Sum	Norm. O	Al	Si	Pb
Kentrolite-(Al)	4	15.29(8)	17.98(1)	66.74(27)	100.02(34)	9	2.00(1)	2.00(1)	2.00(0)
Zoisite-(Pb)	15	19.40(6)	22.76(11)	56.98(37)	99.14(41)	12.5	3.00(1)	2.99(1)	2.02(1)
Lawsonite-(Pb)	11	21.16(29)	25.08(35)	47.47(64)	93.71(1.18)	8	1.99(1)	2.00(1)	1.02(1)
Margarite-(Pb)	16	33.33(1.02)	22.30(0.69)	38.66(1.03)	94.29(2.46)	11	3.79(4)	2.15(3)	1.01(2)
Plumbotsumite	8	1.09(34)	16.32(73)	75.81(1.69)	93.22(1.83)	13	0.30(9)	3.86(10)	4.83(17)
Kentrolite	10	22.00(40)	17.05(12)	62.38(94)	101.43(97)	9	1.98(2)	2.02(2)	1.99(4)
Melanotekite	27	22.07(48)	16.60(26)	61.31(1.47)	99.98(1.43)	9	2.00(4)	2.00(3)	1.99(4)

Note: Synthesis conditions for lawsonite(-Pb) were 4.0 GPa/600 °C.

TABLE 3. Crystal data

Crystal data			
Parameter	$Pb_2Al_2Si_2O_9$	$Pb_2Mn_2Si_2O_9$	$Pb_2Fe_2Si_2O_9$
a (Å)	6.8981(7)	7.0079(4)	6.9788(6)
b (Å)	10.6906(15)	11.0665(5)	11.0164(11)
c (Å)	9.7413(10)	9.9634(5)	10.0881(9)
V (Å^3)	718.37(1)	772.68(8)	775.59(16)
Space group	*Pbcn*	$P2_122_1$	*Pbcn*
Z	4	4	4
Chemical formula	$Pb_2Al_2Si_2O_9$	$Pb_2Mn_2Si_2O_9$	$Pb_2Fe_2Si_2O_9$
D_{calc}	6.15	6.22	6.22
μ (mm^{-1})	47.19	47.25	47.29
Intensity measurements			
Crystal size	Sphere, *r* = 80 μm	150 μm × 200 μm × 80 μm	40 μm × 50 μm × 30 μm
Diffractometer	CCD DETECTOR KM4CCD/SAPPHIRE 3	CCD DETECTOR KM4CCD/SAPPHIRE 3	CCD DETECTOR KM4CCD/SAPPHIRE 3
Monochromator	Graphite	Graphite	Graphite
Radiation	Mo*Kα*, λ = 0.71073	Mo*Kα*, λ = 0.71073	Mo*Kα*, λ = 0.71073
θ-range (°)	3.5–28.0	2.9–28.0	2.9127–28.7128
Reflection range	*h* (–8 ↔ 9), *k* (–12 ↔ 12), *l* (–12 ↔ 11)	*h* (–9 ↔ 10), *k* (–16 ↔ 16), *l* (–14 ↔ 14)	*h* (–9 ↔ 9), *k* (–14 ↔ 12), *l* (–11 ↔ 13)
No. of measured reflections	2386	6934	4577
No. of unique reflections	786	2592	911
No. of observed reflections [$I > 4\sigma(I)$]	674	2256	621
Group, Conditions, Operator	I/s(I)	I/s(I)	I/s(I)
(*h*00), *h* = 2n + 1, 21 ...	0.4	0.8	0.5
(0*k*0), *k* = 2n + 1, ... 21 ...	3.3	12.2	0.3
(00*l*), *l* = 2n + 1, ... 21	1.2	1.8	0.4
(0*kl*), *k* = 2n + 1, b ...	1.0	3.7	0.4
(*h*0*l*), *l* = 2n + 1, ... c ...	1.6	4.5	0.4
(*hk*0), *h* + *k* = 2n + 1, ... n	0.8	5.0	0.4
Refinement of the structures			
No. of parameters used in refinement	72	158	80
R_1 [$F_o > 4\sigma(F_o)$]	0.0223	0.0333	0.0427
R_wR_2 [$F_o > 4\sigma(F_o)$]	0.0494	0.0864	0.0855
Weighting parameter a	0.0391	0.0405 and 2.9347	0.0376
Goodness of fit	1.08	1.13	1.014
Final $\Delta\rho_{min}$ (e/Å^3)	–1.13	–1.75	–3.04
Final $\Delta\rho_{max}$ (e/Å^3)	2.48	2.50	1.96

Note: $R_1 = \Sigma||F_o| - |F_c||/\Sigma|F_o|$, $w = 1/[\sigma^2(F_o^2) + (aP)^2]$, $wR_2 = \{\Sigma[w(F_o^2 - F_c^2)^2]/\Sigma[w(F_o^2)^2]\}$, $P = [2F_c^2 + \max(F_o^2,0)]/3$.

(Spek 2005) yielded 2.4% and *wR*2 for R_1 and *wR*2, respectively. However, this structure refinement has negative U_{iso} for more than 8 atoms, and we dismissed therefore $P2_1cn$ as possible space group for $Pb_2Al_2Si_2O_9$.

The final structure was solved in space group *Pbcn*. All atom positions were found with $R_1 = 5.35\%$. The refinement of the weighting and extinction parameters dropped R_1 to 3.50%. The refinement of the anisotropic displacement factors further reduced R_1 to 2.23%. Two positions with residual electron density (2.48 and 2.18) at a distance of 0.83 and 0.89 Å from the Pb site were found. Fourier-mappings indicate no strong irregularities of the Pb site (Fig. 3) compared with Pb sites of melanotekite and kentrolite. The refined atomic coordinates and equivalent isotropic and anisotropic displacement parameters, as well as selected interatomic distances and angles are given in Tables 5–7.

$Pb_2Mn_2Si_2O_9$

A large (150 × 200 × 80 μm) red crystal of kentrolite was used for structure solution. The λ/2-effect also occurs as in $Pb_2Al_2Si_2O_9$. Lattice parameters were refined on 6934 reflections and yield *a* = 7.0079(4) Å, *b* = 11.0665(5) Å, and *c* = 9.9634(5) Å. An analytical absorption correction was applied. Statistical tests on the |E| values indicated strongly the lack of an inversion center. In contrast to melanotekite and kentrolite-(Al), the extinction law for space group *Pbcn* is violated for (0*kl*) with *k* = 2n + 1, (*h*0*l*) with *l* = 2n + 1, and (*hk*0) with *h* + *k* = 2n + 1.

TABLE 4. Systematic absence violations caused by λ/2-effect for $Pb_2Al_2Si_2O_9$

Regular strong intensities on the basis of (0 4 5) 100%		Observed (*hkl*) not allowed in *Pbcn*	
(2 0 2)	64–70%	(1 0 1)	0.83%
(0 6 2)	22–23%	(0 3 1)	0.26%
(2 8 0)	24%	(1 4 0)	0.16%
(0 6 0)	22%	(0 3 0)	0.29%
(0 0 10)†	61%	(0 0 5)*	0.22%
(0 10 0)	n.d.	(0 5 0)	0.36%

* Intensity was earlier observed by Glasser (1967) and Moore et al. (1991).
† Intensity was mentioned and omitted in the structure solution by Barbier and Lévy (1998).

Only (*h*00) with *h* = 2n + 1 and (00l) with *l* = 2n + 1 extinctions were found and so space group $P2_122_1$ was chosen [$I/\sigma(I) < 2.37$]. Structure solution in this space group results in $R = 7.74\%$.

When we use a higher cutoff $I/\sigma(I) < 6$ for space group determination, we obtain the kentrolite space group $C222_1$ determined earlier by Gabrielson (1961). However, structure solution and refinement in this space group results in an unrealistic structure

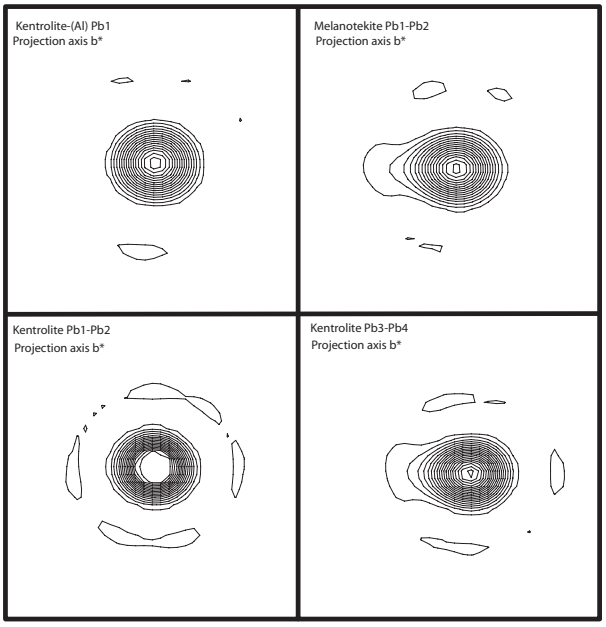

FIGURE 3. Fourier-mappings (F_{obs}) of the Pb sites in kentrolite-(Al), melanotekite, and kentrolite illustrating differences in electron density (16 contour levels with 20 e/Å^3).

model, similar to the one given by Gabrielson (1961), which was characterized by strongly distorted polyhedra, very large thermal-vibration parameters, and high *R*-values. Therefore, this model was not considered.

Based on the lower symmetry of space group $P2_122_1$ two Pb sites, three Mn sites, two Si sites, and ten O sites were located. Additionally, two different residual electron densities of 20 e/Å^3 next to Pb1 and 35 e/Å^3 next to Pb3 were found. We split the two positions in Pb1 and Pb2 with SOF= 0.72 and 0.28, Pb3 and Pb4 with SOF = 0.65 and 0.35, respectively. Structure refinement suggested twinning, and R_w was three times higher than R_1. By the use of the Le Page algorithm (Program Platon, Spek 2005), space group *Pbcn* was indicated with an origin shift of (0 0 0.2498 –0.25) for all atoms with exception of the sites Pb1, Pb2, Pb3, and Pb4. The structure was further refined in twin mode (inversion) with twin fraction 0.42 resulting in $R_1 = 0.033$ and $R_w = 0.086$. Data of the structure and interatomic distances and bond angles are given in Tables 8, 9, and 10.

$Pb_2Fe_2Si_2O_9$

A small (40 × 50 × 30 µm) orange-red crystal of melanotekite was used for single-crystal diffraction studies. No additional peaks caused by λ/2-effect were observed. Lattice parameters were refined on 1298 reflections and yield to $a = 6.9788(6)$ Å, $b = 11.0164(11)$ Å, and $c = 10.0881(9)$ Å. An analytical absorption correction was applied.

Statistical tests on the |E| values indicated strongly the existence of an inversion center, and extinctions were consistent with space group *Pbcn* as in $Pb_2Al_2Si_2O_9$. The *R*-value for this solution was 12.42%. All atoms were found similar as in $Pb_2Al_2Si_2O_9$, however residual electron density of 45 e/Å^3 was located next to the Pb1-site. On that position we added a Pb2-atom with SOF 0.3 and reduced the SOF of Pb1 to 0.7, following the method used by Moore et al. (1991). The refinement of the anisotropic displacement factors and weighting parameters reduced agreement values to $R_1 = 4.28\%$ and $R_w = 8.56\%$. Additional refinements of the Pb-SOF with constraints between Pb1 and Pb2 did not significantly improve *R*-values and often resulted in negative anisotropic displacement factors for O1 and Pb2. The refined

TABLE 5. $Pb_2Al_2Si_2O_9$—Fractional atomic coordinates and equivalent isotropic displacement parameters (Å^2)

Atom	Ox. state	M, Wyckoff letter	*x*	*y*	*z*	U_{eq}	SOF
Pb1	Pb+2	8*d*	0.45060(4)	0.30435(3)	0.54954(3)	0.0123(2)	1
Al1	Al+3	4*b*	0.5	0	0	0.006(1)	1
Al2	Al+3	4*c*	0.5	0.1467(3)	0.25	0.007(1)	1
Si1	Si+4	8*d*	0.2171(3)	–0.0883(2)	0.2488(2)	0.007(1)	1
O1	O-2	8*d*	0.3477(6)	0.0082(4)	0.3372(5)	0.008(1)	1
O2	O-2	8*d*	0.3080(7)	–0.1068(5)	0.0965(5)	0.011(1)	1
O3	O-2	8*d*	0.1854(6)	–0.2260(5)	0.3169(5)	0.009(1)	1
O4	O-2	4*c*	0	–0.0227(7)	0.25	0.010(1)	1
O5	O-2	8*d*	0.6096(7)	0.1410(5)	0.4230(5)	0.008(1)	1

TABLE 6. $Pb_2Al_2Si_2O_9$—Anisotropic thermal-vibration parameters (×10^4)

	U_{11}	U_{22}	U_{33}	U_{23}	U_{13}	U_{12}
Pb1	137(2)	153(2)	79(2)	–10(1)	–6(1)	–1(1)
Al1	50(12)	104(17)	21(13)	–1(11)	–3(10)	14(12)
Al2	66(12)	108(17)	27(13)	0	–12(11)	0
Si1	53(8)	129(11)	36(8)	5(7)	1(6)	–9(7)
O1	79(20)	142(27)	32(21)	5(19)	9(19)	–6(20)
O2	147(24)	138(29)	38(20)	–21(19)	31(19)	–39(20)
O3	80(22)	103(27)	96(24)	7(18)	13(19)	–36(19)
O4	49(29)	77(39)	180(37)	0	–7(29)	0
O5	66(21)	122(27)	38(21)	7(18)	–18(18)	–13(20)

TABLE 7. $Pb_2Al_2Si_2O_9$—Selected interatomic distances (Å) and bond angles (°)

	M1	Angle (°)		**M2**	Angle (°)
2×	Al1-O5	1.846(5)	2×	Al2-O5	1.848(4)
2×	Al1-O1	1.905(5)	2×	Al2-O3	1.978(5)
2×	Al1-O2	1.985(5)	2×	Al2-O1	2.004(5)
	Average	1.912(5)		Average	1.943(5)
2×	O1-Al1-O5	81.35(19)	2×	O1-Al2-O5	78.67(21)
2×	O2-Al1-O5	89.77(22)	2×	O3-Al2-O5	89.24(22)
2×	O1-Al1-O2	89.99(19)	1×	O1-Al2-O1	84.74(29)
2×	O1-Al1-O2	90.01(19)	2×	O3-Al2-O5	93.37(22)
2×	O1-Al1-O5	98.65(19)	2×	O1-Al2-O3	91.71(19)
2×	O2-Al1-O5	90.23(22)	2×	O1-Al2-O5	98.49(23)
	Average	90.00(20)	1×	O3-Al2-O3	93.06(31)
				Average	90.06(23)
	T1			**A1**	
1×	Si1-O1	1.618(5)		Pb1-O2	2.375(5)
1×	Si1-O2	1.622(5)		Pb1-O5	2.402(5)
1×	Si1-O3	1.630(5)		Pb1-O5	2.439(5)
1×	Si1-O4	1.654(3)		Pb1-O3	2.474(5)
	Average	1.631(5)			
				Pb1-O2	3.001(5)
				Pb1-O3	2.950(5)
				Pb1-O4	3.063(5)
1×	O1-Si1-O4	103.29(26)			
1×	O3-Si1-O4	104.96(27)			
1×	O2-Si1-O3	108.32(28)		**[PbAlO]-cluster**	
1×	O1-Si1-O2	110.43(25)		Al2-O5-Al1	103.30(26)
1×	O2-Si1-O4	114.09(20)		Pb1-O5-Al1	101.44(20)
1×	O1-Si1-O3	115.74(25)		Pb1-O5-Al1	123.10(23)
	Average	109.47(25)		Pb1-O5-Pb1	104.91(23)
				Pb1-O5-Pb1	119.12(22)
				Pb1-O5-Pb1	102.12(19)
				Average	109.0(2)

TABLE 8. $Pb_2Mn_2Si_2O_9$—Fractional atomic coordinates and equivalent isotropic displacement parameters (Å^2)

Atom	Ox. state	M, Wyckoff letter	x	y	z	U_{eq}	SOF
Pb1	Pb+2	4*c*	0.5486(3)	0.5525(2)	0.2001(3)	86(3)	0.72
Pb2	Pb+2	4*c*	0.5348(9)	0.5476(5)	0.1989(10)	267(16)	0.28
Pb3	Pb+2	4*c*	0.5479(2)	–0.0599(3)	0.2974(3)	95(2)	0.65
Pb4	Pb+2	4*c*	0.4986(4)	–0.0558(5)	0.2985(7)	245(8)	0.35
Mn1	Mn+3	2*b*	0.5000	0.1048(2)	0.0000	68(4)	1
Mn2	Mn+3	2*a*	0.0000	0.6054(2)	0.0000	63(4)	1
Mn3	Mn+3	4*c*	0.5016(2)	0.2490(1)	0.2496(1)	69(3)	1
Si1	Si+4	4*c*	0.7876(4)	0.1571(2)	0.4971(3)	87(5)	1
Si2	Si+4	4*c*	0.7867(4)	0.3436(2)	–0.0037(2)	69(5)	1
O1	O-2	4*c*	0.8887(10)	0.6092(5)	0.1731(5)	99(12)	1
O2	O-2	2*b*	0.0000	0.2222(8)	0.5000	212(25)	1
O3	O-2	4*c*	0.7009(11)	0.3679(5)	0.1434(6)	115(13)	1
O4	O-2	4*c*	0.8122(11)	0.4729(6)	–0.0808(6)	134(13)	1
O5	O-2	4*c*	0.7901(13)	–0.1351(6)	0.1474(6)	193(17)	1
O6	O-2	4*c*	0.6634(11)	0.2454(5)	–0.0882(6)	102(12)	1
O7	O-2	4*c*	0.8117(10)	0.0266(6)	0.4218(6)	112(13)	1
O8	O-2	4*c*	0.6566(11)	0.2511(5)	0.4152(6)	106(13)	1
O9	O-2	4*c*	0.6148(10)	0.1107(5)	0.1720(6)	93(12)	1
O10	O-2	2*a*	0.0000	0.2811(8)	0.0000	145(21)	1

atomic coordinates and equivalent isotropic and anisotropic displacement parameters, as well as selected interatomic distances and angles are given in Tables 11–13.

TABLE 9. $Pb_2Mn_2Si_2O_9$—Anisotropic thermal-vibration parameters (×10^4)

	U_{11}	U_{22}	U_{33}	U_{23}	U_{13}	U_{12}	U_{eq}
Pb1	91(4)	77(5)	90(6)	11(5)	–15(4)	40(4)	86(3)
Pb2	435(29)	192(17)	173(20)	12(15)	–26(21)	–213(13)	267(16)
Pb3	83(5)	107(3)	95(3)	11(3)	9(5)	–12(4)	95(2)
Pb4	444(21)	163(9)	127(7)	4(8)	–13(20)	–98(17)	245(8)
Mn1	70(9)	75(7)	59(7)	0	–4(6)	0	68(4)
Mn2	55(9)	73(7)	62(7)	0	16(6)	0	63(4)
Mn3	75(6)	68(5)	64(5)	–8(4)	–6(4)	–1(4)	69(3)
Si1	83(13)	94(10)	84(10)	–3(9)	–16(8)	16(11)	87(5)
Si2	58(12)	72(9)	77(10)	–3(9)	5(8)	12(11)	69(5)
O1	96(30)	141(26)	61(26)	1(19)	–17(23)	5(26)	99(12)
O2	34(47)	57(39)	544(71)	0	–120(46)	0	212(25)
O3	159(36)	89(27)	99(27)	–70(21)	60(27)	–49(28)	115(13)
O4	163(35)	114(28)	125(28)	36(24)	67(26)	–23(29)	134(13)
O5	372(50)	119(30)	88(28)	–36(24)	–38(32)	90(34)	193(17)
O6	86(31)	114(28)	108(28)	–1(23)	–11(25)	–47(25)	102(12)
O7	75(29)	89(26)	174(30)	–47(24)	–12(25)	5(26)	112(13)
O8	102(32)	138(28)	79(27)	–3(23)	4(24)	34(26)	106(13)
O9	86(29)	119(25)	73(26)	2(19)	–22(22)	–23(25)	93(12)
O10	75(50)	67(37)	294(52)	0	16(38)	0	145(21)

DISCUSSION

Lattice parameter

The lattice parameters of $Pb_2Al_2Si_2O_9$ are very small compared to other kentrolite isotypes and its cell volume is the smallest ever observed in the kentrolite structure family. The lattice parameters of the Al, Ga, and In end-members are a linear function of their ionic radii (Fig. 4). Unit-cell volume of kentrolite and melanotekite show the same trend when sixfold-coordinated Mn^{3+} and Fe^{3+} is present in high spin mode with ionic radii of 0.645 Å (Shannon 1976). Lattice parameters *a* and *b* are slightly higher in kentrolite, whereas *c* is obviously shorter than in melanotekite.

Space groups of the kentrolite structure family

The structure model of melanotekite and kentrolite-(Al) in space group *Pbcn* is in good agreement with the structure model of Moore et al. (1991).

The observed λ/2-effect for kentrolite-(Al) causes further weak intensities [(005), (101), (031)], which violate the extinction law of *Pbcn* and makes space group determination for kentrolite structures in general more complicated. Based on our results for kentrolite-(Al) and kentrolite, we speculate that λ/2-effect of the strong (0010) reflection is most likely the reason for the (005)-reflection earlier observed by Glasser (1967) and Moore et al. (1991).

In the structure of the analyzed kentrolite crystal, lead atoms do not conform to space group *Pbcn* as the rest of the structure (see electron density maps in Fig. 5). As a result, glide planes, inversion center and 2_1 screw axis along **b** are lost. Therefore, $P2_122_1$ is the most reasonable space group for our synthetic kentrolite crystals and not $C222_1$ as suggested by Gabrielson (1961).

There are three space groups *Pbcn*, $P2_122_1$, and $P2_1cn$ in the kentrolite structure family. Melanotekite and kentrolite-(Al), kentrolite, and kentrolite-(In) have a different cation on the M site and were obtained by different synthesis conditions. The In end-member with large M-octahedra and lattice volume was obtained from high-temperature experiments, whereas the Al end-member with small M-octahedra and small lattice volume was obtained by high-pressure experiments. We generally assume that lattice volume of kentrolite increases with temperature and that could result in changes of the Pb site, which might influence symmetry. The observed split of Pb sites in the kentrolite structure family is possibly a result of thermal treatment similar as in feldspar-(Pb) (Tribaudino et al. 1998). Based on the split Pb sites and the observed pseudo symmetry to *Pbcn*, we speculate that with increase in temperature at least one phase transition occurs in kentrolite, with change of space group from $P2_122_1$ to *Pbcn*.

Structure

The linkage of T- and M-polyhedra of the refined crystal structures is generally identical with the structure described by Moore et al. (1991), Barbier and Lévy (1998), and Werner and Müller-Buschbaum (1997). To compare the structures visually, the Figure 6 shows a projection along **c** on the **a-b** plane of each end-member. From this view, structures are nearly identical with exception of the lead position. In the kentrolite structure, two different and split Pb sites are laterally linked to the octahedral chain and alternate along the **b**-axes.

TABLE 10. $Pb_2Mn_2Si_2O_9$—Selected interatomic distances (Å) and bond angles (°)

Bond length			O-M-O angles		
	A1	(Å)		**M1**	Angle (°)
	Pb1-O3	2.373(7)		O6′-Mn1-O6	85.73(36)
	Pb1-O4	2.407(7)		O7-Mn1-O7	93.01(34)
	Pb1-O1	2.460(6)	2×	O6-Mn1-O9	80.18(26)
	Pb1-O1	2.479(7)	2×	O6′-Mn1-O9	96.93(25)
	Average	2.430(7)	2×	O7′-Mn1-O9	87.42(25)
			2×	O6-Mn1-O7	90.84(25)
	A1′		2×	O7′-Mn1-O9′	95.27(26)
	Pb2-O3	2.370(8)			90.00(27)
	Pb2-O1	2.384(10)			
	Pb2-O4	2.454(11)		**M2**	
	Pb2-O1	2.585(10)		O4′-Mn2-O4	92.89(37)
	Average	2.448(10)		O8′-Mn2-O8″	82.19(36)
			2×	O4′-Mn2-O8″	92.62(26)
	A2		2×	O8′-Mn2-O1′	80.38(25)
	Pb3-O9	2.311(6)	2×	O8″-Mn2-O1′	97.72(26)
	Pb3-O5	2.409(8)	2×	O4′-Mn2-O1′	96.01(26)
	Pb3-O7	2.422(7)	2×	O4-Mn2-O1′	85.72(26)
	Average	2.381(7)			90.00(28)
	A2′			**M3**	
	Pb4-O9	2.375(8)		O8-Mn3-O9	96.93(26)
	Pb4-O7	2.576(9)		O6′-Mn3-O9	84.04(26)
	Pb4-O5	2.624(9)		O3-Mn3-O9	91.20(26)
	Pb4-O7	2.675(8)		O5′-Mn3-O9	90.53(27)
	Pb4-O5	2.685(10)		O8-Mn3-O1′	83.23(26)
	Average	2.587(9)		O6′-Mn3-O1′	95.83(25)
				O3-Mn3-O1′	88.02(25)
	M1			O5′-Mn3-O1′	90.23(28)
2x	Mn1-O9	1.894(6)		O3-Mn3-O8	92.63(27)
2x	Mn1-O7	2.113(7)		O5′-Mn3-O8	89.31(29)
2x	Mn1-O6	2.122(6)		O3-Mn3-O6′	89.51(26)
	Average	2.043(6)		O5′-Mn3-O6′	88.48(29)
					90.00(27)
	M2				
2x	Mn2-O1	1.894(6)		O-T-O angles	
2x	Mn2-O8	2.107(6)		**T1**	
2x	Mn2-O4	2.129(7)		O5-Si1-O8	112.08(39)
	Average	2.043(6)		O7-Si1-O8	113.37(35)
				O2-Si1-O8	103.92(37)
	M3			O7-Si1-O5	109.14(35)
	Mn3-O9	1.890(6)		O2-Si1-O5	110.69(34)
	Mn3-O1	1.919(6)		O2-Si1-O7	107.45(39)
	Mn3-O8	1.975(6)		Average	109.44(37)
	Mn3-O6	1.981(7)			
	Mn3-O3	2.192(7)		**T2**	
	Mn3-O5	2.200(7)		O6-Si2-O3	112.70(36)
	Average	2.026(7)		O4-Si2-O3	108.86(33)
				O10-Si2-O3	112.94(30)
	T1			O4-Si2-O6	113.59(34)
	Si1-O8	1.610(7)		O10-Si2-O6	102.31(37)
	Si1-O5	1.612(7)		O10-Si2-O4	106.21(39)
	Si1-O7	1.636(6)		Average	109.44(35)
	Si1-O2	1.654(5)			
	Average	1.628(6)			
				[PbMnO]-cluster	
	T2			Mn3-O1-Mn2	102.3
	Si2-O3	1.606(6)		Mn2-O1-Pb1	119.3
	Si2-O6	1.624(7)		Pb1-O1-Mn3	124.0
	Si2-O4	1.634(7)		Mn3-O1-Pb2	101.8
	Si2-O10	1.647(5)		Pb2-O1-Pb1	99.8
	Average	1.628(6)		Mn2-O1-Pb2	107.1
				Average	109.1
				[PbMnO]-cluster	
				Pb4-O9-Mn1	120.0
				Pb4-O9-Mn3	122.8
				Mn3-O9-Mn1	102.7
				Mn1-O9-Pb3	112.0
				Pb3-O9-Mn3	110.8
				Pb3-O9-Pb4	87.7
				Average	109.3

TABLE 11. $Pb_2Fe_2Si_2O_9$—Fractional atomic coordinates and equivalent isotropic displacement parameters (Å²)

Atom	Ox. state	M, Wyckoff letter	x	y	z	U_{eq}	SOF
Pb1	Pb+2	8*d*	0.4482(2)	0.3016(2)	0.5494(3)	104(3)	0.7
Pb2	Pb+2	8*d*	0.5121(6)	0.3088(6)	0.5499(6)	300(11)	0.3
Fe1	Fe+3	4*b*	0.5	0	0	70(6)	1
Fe2	Fe+3	4*c*	0.5	0.1521(3)	0.25	73(6)	1
Si1	Si+4	8*d*	0.2151(4)	−0.0864(4)	0.2503(3)	62(8)	1
O1	O-2	8*d*	0.3414(10)	0.0109(8)	0.3347(7)	73(19)	1
O2	O-2	8*d*	0.3039(12)	−0.1083(9)	0.1019(8)	128(22)	1
O3	O-2	8*d*	0.1915(10)	−0.2201(9)	0.3227(8)	121(22)	1
O4	O-2	4*c*	0	−0.0244(13)	0.25	199(32)	1
O5	O-2	8*d*	0.6146(11)	0.1481(9)	0.4259(8)	114(20)	1

TABLE 12. $Pb_2Fe_2Si_2O_9$—Anisotropic thermal-vibration parameters ($\times 10^4$)

	U_{11}	U_{22}	U_{33}	U_{23}	U_{13}	U_{12}
Pb1	79(5)	114(5)	120(4)	−18(5)	−11(6)	−12(5)
Pb2	652(30)	140(17)	108(12)	20(14)	−3(29)	140(27)
Fe1	91(11)	52(14)	69(11)	−5(12)	−12(9)	10(9)
Fe2	80(12)	81(13)	59(12)	0	6(9)	0
Si1	33(15)	72(19)	81(16)	32(18)	−17(12)	−12(14)
O1	104(39)	43(50)	73(45)	40(46)	−9(32)	−14(35)
O2	158(45)	131(58)	96(48)	−18(48)	53(34)	−32(36)
O3	85(40)	159(62)	118(48)	−12(47)	9(32)	−38(33)
O4	50(56)	146(79)	400(84)	0	−50(54)	0
O5	111(42)	148(50)	83(47)	27(42)	5(35)	−49(37)

TABLE 13. $Pb_2Fe_2Si_2O_9$—Selected interatomic distances (Å) and bond angles (°)

	M1	Angle (°)		**M2**	Angle (°)
2×	Fe1-O5	1.965(9)	2×	Fe2-O5	1.947(8)
2×	Fe1-O1	2.005(7)	2×	Fe2-O3	2.075(9)
2×	Fe1-O2	2.086(9)	2×	Fe2-O1	2.092(8)
	Average	2.019(8)		Average	2.038(8)
2×	O1-Fe1-O5	81.89(32)	2×	O1-Fe2-O5	97.94(35)
2×	O2-Fe1-O5	88.85(37)	2×	O3-Fe2-O5	87.58(35)
2×	O1-Fe1-O2	90.76(32)	1×	O1-Fe2-O1	83.93(45)
2×	O1-Fe1-O2	89.24(32)	2×	O3-Fe2-O5	94.18(33)
2×	O1-Fe1-O5	98.11((32)	2×	O1-Fe2-O3	91.12(33)
2×	O2-Fe1-O5	91.15(37)	2×	O1-Fe2-O5	80.11(32)
	Average	90.00(34)	1×	O3-Fe2-O3	94.51(51)
				Average	90.03(36)
	T1			**Pb1**	
1×	Si1-O1	1.628(8)		Pb1-O2	2.415(10)
1×	Si1-O2	1.638(9)		Pb1-O5	2.401(9)
1×	Si1-O3	1.652(10)		Pb1-O5	2.406(8)
1×	Si1-O4	1.649(7)		Pb1-O3	2.498(9)
	Average	1.642(8)			
				Pb2	
				Pb2-O5	2.238(11)
				Pb2-O3	2.625(10)
1×	O1-Si1-O4	102.75(49)		Pb2-O2	2.696(11)
1×	O3-Si1-O4	106.18(49)		Pb2-O2	2.707(10)
1×	O2-Si1-O3	108.14(49)		Pb2-O3	2.715(10)
1×	O1-Si1-O2	111.72(44)			
1×	O2-Si1-O4	113.80(37)		**[PbFeO]-cluster**	
1×	O1-Si1-O3	114.18(44)		Fe1-O5-Fe2	101.42(39)
	Average	109.46(45)		Pb1-O5-Fe2	104.96(38)
				Pb1-O5-Fe2	119.11(38)
				Pb1-O5-Fe1	100.99(33)
				Pb1-O5-Pb1	123.10(40)
				Pb1-O5-Pb1	104.61(34)
				Average	109.0(4)

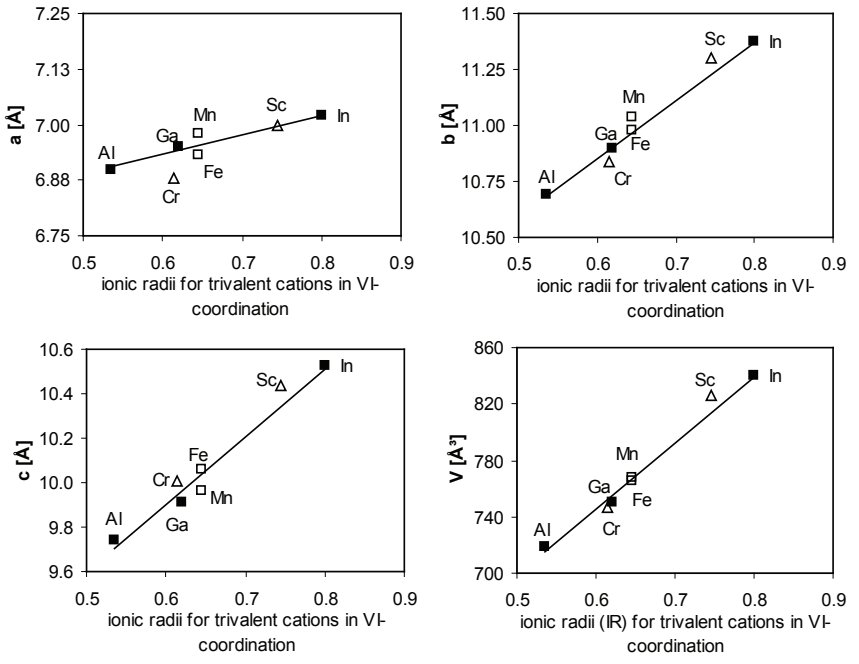

FIGURE 4. Changes in lattice parameters as a function of ionic radii (Shannon 1976) of trivalent cations (Fe, Mn in high spin) on the M-positions in sixfold coordination in kentrolite isotypes. Open squares represent data for melanotekite and kentrolite (this study); filled squares represent the kentrolite isotypes of Al, In, and Ga (Al = this study; In = Werner and Müller-Buschbaum 1997; Ga = Gabelica-Robert and Tarte 1979) open triangles represent Cr and Sc-isotypes (Gabelica-Robert and Tarte 1979).

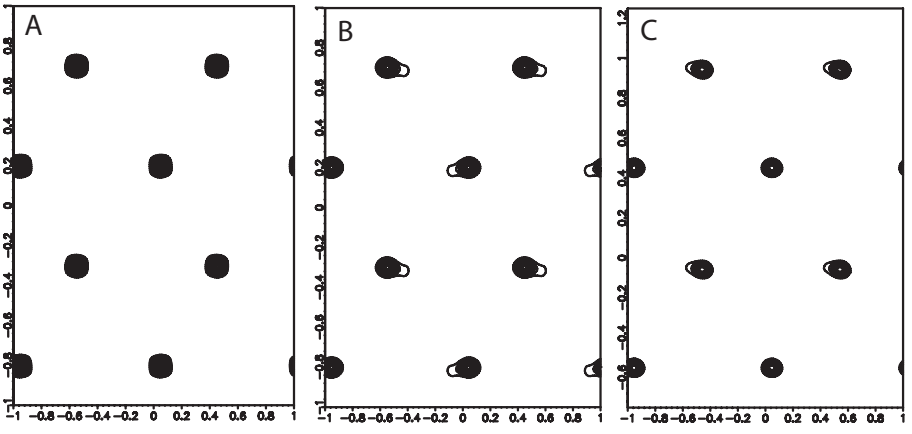

FIGURE 5. Fourier maps (F_{obs}) with projection from **c** on the **a-b** plane, Pb-positions are shown for kentrolite-(Al) in *Pbcn* (**a**), melanotekite in *Pbcn* (**b**) and kentrolite in $P2_122_1$ (**c**).

Octahedra chain

Kinked octahedra chains of melanotekite, kentrolite, and kentrolite-(Al) are very similar. Only small differences occur in M2-M2-M2 angles within the chain. The smaller octahedra chain of the Al-isotype and kentrolite is more stretched than in the In-isotype (Al2-Al2-Al2 = 114.4°, and Mn1-Mn2-Mn1 = 114.5°, Fe2-Fe2-Fe2 = 112.81°, In2-In2-In2 = 110.2°, see Fig. 7). The decrease in M2-M2-M2 angle and kinking of M2-M1-M2 sequence is linked to the size of each octahedron and the fixed distance O1-O2, the edge of the T1.

In kentrolite-(Al) the Al1-Al2-Al1 = 180.00°, melanotekite Fe2-Fe1-Fe2 = 179.98°, and kentrolite Mn1-Mn3-Mn2 = 179.54°. The octahedra volumes and edges O3-O3 in $Pb_2Al_2Si_2O_9$ (2.87 Å) and $Pb_2Fe_2Si_2O_9$ (3.05 Å) and O7-O7 and O4-O4 in $Pb_2Mn_2Si_2O_9$ (3.07 and 3.09 Å, respectively) increase in the order Al, Fe, and Mn (Table 14).

Beyond the size of M-octahedra, there are no pronounced differences in the M1 and M2 octahedra of kentrolite-(Al) and melanotekite. The ratio of the bond-length M1-O5, M1-O1, and M1-O2 is 0.97:1.00:1.04 in kentrolite-(Al) and 0.98:1.00:1.04 in melanotekite. The ratio of the bond-length M2-O5, M2-O3, and M2-O1 is 0.93:1.00:1.01 in kentrolite-(Al) and 0.94:1.00:1.01 in melanotekite.

Some significant differences are noted for kentrolite. The ratio of the bond-length is for M1-O9, M1-O7, and M1-O6 0.90:1.00:1.00 and for M2-O1, M2-O8, and M2-O4 0.90:1.00:1.01. The octahedral sites M1 and M2 in kentrolite are tetragonally (2 + 4)-distorted, what is commonly observed for $Mn^{3+}O_6$ octahedra (Jahn-Teller effect). The M3 octahedron behaves differently. Here, we have two short, two intermediate, and two long M3-O bonds with the ratio 0.96:1.00:1.11 (see Table 10 and Figs. 7c and 7d). Mn1-O9 and Mn2-(O1) are perpendicular to **b** crystallographic axis and roughly parallel to **c**, therefore **c** in kentrolite is shortened compared to that in melanotekite, whereas **a** and **b** are stretched due to the increased equatorial bond lengths Mn1-O7, Mn1-O6, Mn2-O4, Mn2-O8, Mn3-O5,

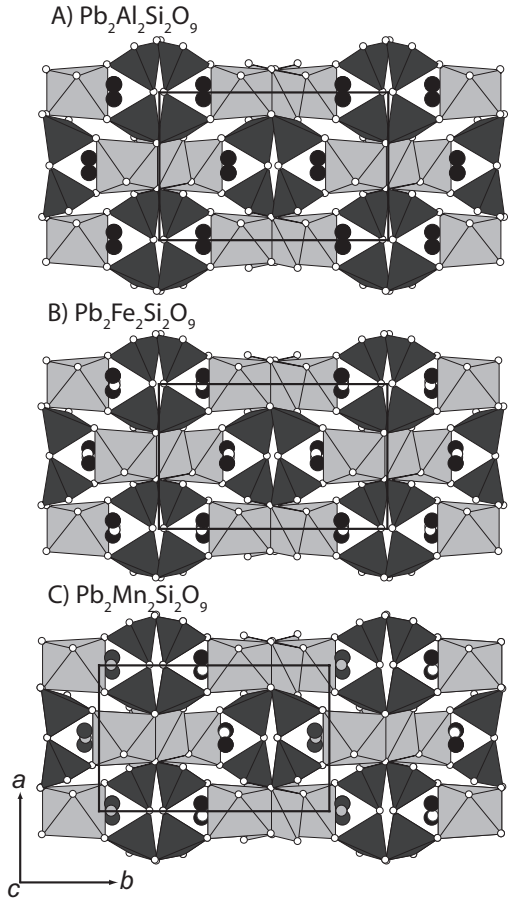

FIGURE 6. Crystal structure of (**a**) kentrolite-(Al), (**b**) melanotekite, and (**c**) kentrolite, projected from **c** on the **a-b** plane. Lead positions with high site occupation factor (SOF) are shown as black and gray filled circles. Split lead positions with low SOF are shown as small white or gray filled circles.

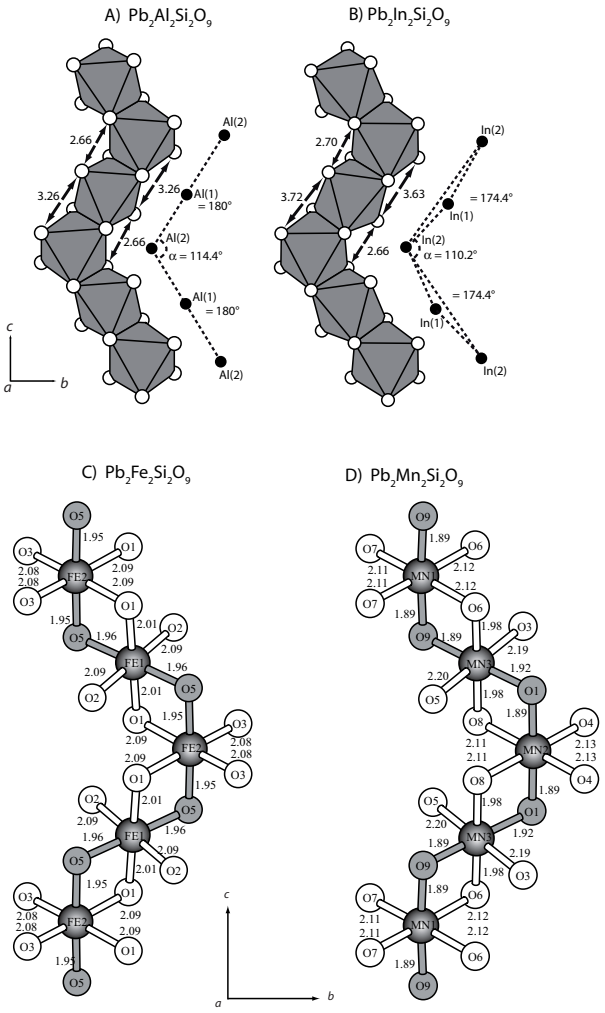

FIGURE 7. Differences in octahedral chain in (**a**) kentrolite-(Al) compared to (**b**) kentrolite-(In). Octahedra chain in kentrolite-(Al) is stretched. Black dots represent Al1 and Al2 atoms in kentrolite-(Al), respectively, In1 and In2 atoms in Kentrolite-(In). Differences in M-octahedra of (**c**) melanotekite and (**d**) kentrolite is shown with bond-length. The shortest bonds of each octahedon are in gray.

TABLE 14. Polyhedra volume, quadratic elongation, and angle variance of $Pb_2M_2Si_2O_9$ (M = Al, Mn, Fe)

Source	This work	This work	This work	Moore et al. (1991)
Polyhedra	$Pb_2Al_2Si_2O_9$	$Pb_2Mn_2Si_2O_9$	$Pb_2Fe_2Si_2O_9$	$Pb_2(Fe_{0.64},Mn_{1.36})Si_2O_9$
volume (Å^3)				
M1	9.199	11.153	10.842	10.728
M2	9.583	11.099	11.078	10.854
M3		10.953		
T1	2.206	2.205	2.253	2.192
T2		2.197		
Quadratic elongation λ				
M1	1.009	1.016	1.008	1.010
M2	1.015	1.019	1.014	1.019
M3		1.012		
T1	1.006	1.003	1.005	1.004
T2		1.006		
Angle Variance σ^2				
M1	27.23	35.12	24.64	22.637
M2	42.51	45.12	38.89	44.43
M3		15.96		
T1	24.26	11.71	20.76	17.03
T2		22.66		

and Mn3-O3. Octahedra distortions are $\Delta_{M1} = 0.003$, $\Delta_{M2} = 0.003$, and $\Delta_{M3} = 0.004$ with $\Delta_M = 1/6\ \Sigma[(L_i - L_m)/L_m]^2$ (L_i is an individual Mn^{3+}-O bond-length and L_m is the mean Mn^{3+}-O bond-length of the corresponding octahedron, see Table 10). The Δ_{M3} value fits well with the dependence of mean distance on distortion given by Shannon et al. (1975) and Burns et al. (1994). However, Δ_{M1} and Δ_{M2} values do not conform to these trends.

In Figure 8, we compare the sizes of the M-octahedra in the Al- and In-isotypes with the sizes of the simple oxides (M_2O_3) of the third group of the periodic table of the elements. Both M1 and M2-octahedra of the Al-isotype are larger than in the corresponding α-Al_2O_3, and both octahedra of the In-isotype are smaller than in In_2O_3. If a solid solution between these isotypes or with the Ga-isotype exists, the M1-site is most likely preferred by atoms with larger ionic radii and the M2-site by those with smaller ionic radii.

(PbMO)-cluster

In melanotekite and kentrolite-(Al) the atom closest to Pb is O5 and in kentrolite it is O9 and O1. Within the octahedra, M1-O5 and M2-O5 distances are also much smaller than the other octahedral distances in melanotekite. In kentrolite, distances Mn1-O9, Mn2-O1, Mn3-O9, and Mn3-O1 behave in the same way.

The O5 atom in kentrolite-(Al) and melanotekite, and also the O1 and O9 atoms in kentrolite are therefore more strongly bonded by Pb and the M sites than any other O atom in the kentrolite structure. For melanotekite and kentrolite-(Al), the O5-atom is fourfold-coordinated by two Pb^{2+} and two Fe^{3+} cations, and O5 is located in a stretched tetrahedron. The same applies to kentrolite for atoms O1 and O9. The tetrahedra are linked with each other over all vertices and build a 3D-network. In Figure 9, the melanotekite structure is plotted with Si_2O_7-groups and the (PbFeO)-cluster projected from **a** on the **b-c** plane. From this view Si_2O_7-groups are located in the middle of (PbFeO)-cluster "6-er" rings with (Fe, Fe, Fe, Pb, Fe, Pb) linkage sequence. The Fe-O and Pb-O bonds, which influence the position of the Si_2O_7-group, are drawn in as solid black and white lines. The fact that two short Fe1-O5 and two short Fe2-O5 distances occur results in weaker Fe-O bonds to oxygen atoms of the Si_2O_7-group, which might cause the high-spin mode of Fe^{3+} and Mn^{3+}.

Si_2O_7-group

The oxygen positions and symmetry of the Si_2O_7-group are influenced strongly by M2, because the O3-O3 distance of the opposing tetrahedron is also an edge of one M2 octahedron. When the size of the octahedra increases, the angle Si1-O4-Si1 will also increase. The small octahedra in $Pb_2Al_2Si_2O_9$ causes a Si1-O4-Si1 angle of 129.84° for the Si_2O_7-group; this angle is 131.08° in melanotekite. In kentrolite two different Si_2O_7 groups are present with angles Si1-O2-Si1 = 128.34° and Si2-O(10)-Si2 = 130.33°.

The corresponding Si1-O6-Si1 angle of the Si_2O_7-group of $Pb_2In_2Si_2O_9$ (Werner and Müller-Buschbaum 1997) is about 134°. The obtained Si-O-Si angles in this work are in total agreement with IR and Raman studies on the kentrolite group by Gabelica-Robert and Tarte (1979). In addition to that they found only one $\nu_{sym.}$ (SiOSi)-frequency at 696 cm^{-1} in melanotekite but two $\nu_{sym.}$ (SiOSi)-frequencies at 701 cm^{-1} and 694 cm^{-1} in synthetic kentrolite. This can be explained by two different Si_2O_7-groups in the kentrolite structure model in space group $P2_122_1$.

Pb site

As shown in the Fourier maps for melanotekite and kentrolite, electron density distribution at the Pb site is very inhomogeneous. This results in additional electron densities of 20–40 e/Å^3, 0.5–0.7 Å away from the Pb site, conspicuous in the structure refinement procedure. The split into two Pb sites in melanotekite and kentrolite reduce residual electron densities below 3. In the refinement of both split Pb sites, their displacement spheres interpenetrate because they are very close to each other. In melanotekite, the distance between the split Pb site is Pb1-Pb2 = 0.45 Å, and in kentrolite distances are Pb1-Pb2 = 0.11 Å, Pb3-Pb4 = 0.35 Å. The interpenetration can result in erroneous thermal-vibration parameters for the split positions and might influence also other atoms.

The lead position in kentrolite-(Al) can be compared with the lead position in massicot (PbO). In $Pb_2Al_2Si_2O_9$, lead has four next O-atoms with Pb-O distances of 2.37–2.47 Å on one side and three further oxygen atoms on the other side with Pb-O distances of 2.95–3.06 Å. The lone electron pair of Pb^{2+} is invisible in the electron density maps. However, it is thought to lie along the Pb-O5 vector in in kentrolite-(Al) and melanotekite and along the Pb-O1 or Pb-O9 vector in kentrolite, respectively.

Bond valence calculations for Pb site show that this position is deficient in bond valence (s = 1.71, instead of 2.00). Atom O3, which is also influenced by the Pb site is also somewhat low in bond valence (s = 1.76, instead of 2.00). In melanotekite,

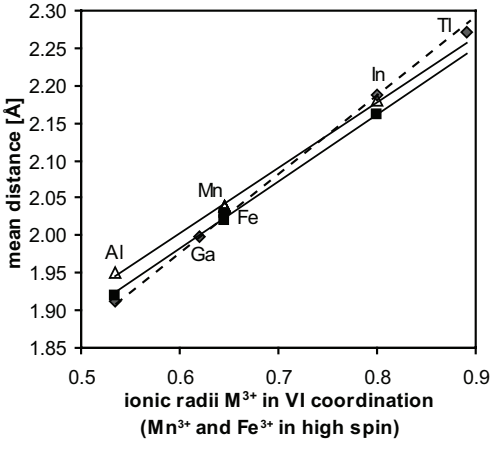

FIGURE 8. Comparison of mean M-O distances of M^{3+} (M = Al, Ga, In, Tl) octahedra in $Pb_2M_2Si_2O_9$ and M_2O_3 as a function of ionic radii (Shannon 1976).

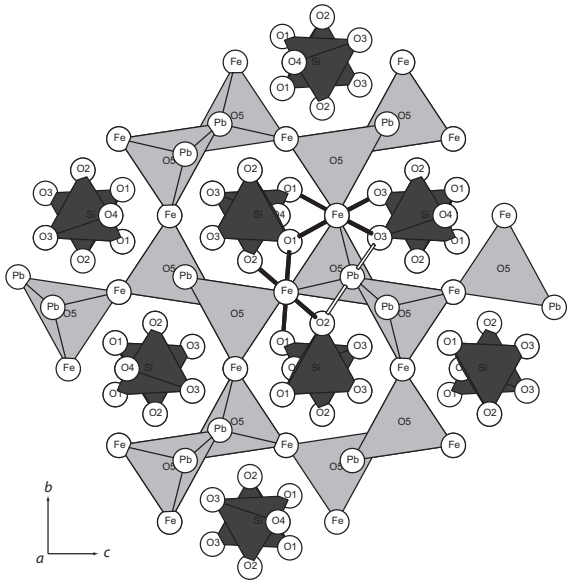

FIGURE 9. Projection of the melanotekite structure from **a** on the **b-c** plane. (PbFe)O-cluster with O5 as central atom builds a 3D-network. The Si_2O_7-group is placed in cavities of the cluster-network. Additional Fe-O and Pb-O bonds are shown as solid black and white lines, respectively.

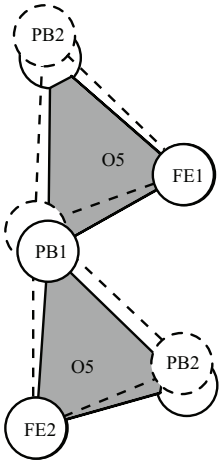

FIGURE 10. [PbFeO]-cluster displacement by split Pb site.

Pb1 has four next neighbors as kentrolite-(Al) and is placed between two octahedral chains, bonded by two O5 atoms with same strength. The split partner Pb2 is shifted toward one of these O5 atoms and has in total one very short bond with O5 and four intermediate bonds with O3 and O2. The split of the lead position can also described as a stretching of (PbFeO)-clusters (Fig. 10). In kentrolite, Pb1 is bonded with four oxygen atoms (O1, O1, O3, and O4), and it is rotated toward O3. The split partner Pb2 is slightly shifted between O3 and O1 similar to the Pb2 in melanotekite. Pb3 and Pb4 behave differently. Pb3 is very strongly bonded to O9 and has in total three next nearest oxygen neighbors with O5 and O7. The split partner Pb4 has five next-nearest O neighbors O9 and two times O5 and O7. Pb4 is more symmetrically placed between the two O5 and O7 atoms and shifted away from O9.

ACKNOWLEDGMENTS

This work was supported by the DFG, Project FR 557/18. We thank Marina Borowski and Elisabeth Irran (Anorganische Chemie, TU-Berlin, Germany) for their support at the single-crystal diffractometer as well as François Galbert (ZELMI, TU-Berlin, Germany) for his help at the microprobe.

REFERENCES CITED

Altomare, A., Cascarano, G., Giacovazzo, C., Guagliardi, A., Burla, M.C., Polidori, G., and Camalli, M. (1992) SIR92—a program for automatic solution of crystal structures by direct methods. Journal of Applied Crystallography, 27, 435.

Anastasiou, P. and Langer, K. (1977) Synthesis and physical properties of piemontite $Ca_2Al_{3p}Mn^{3+}_p(Si_2O_7/SiO_4/O/OH)$. Contribution to Mineralogy and Petrology, 60, 225–245.

Barbier, J. and Lévy, D. (1998) $Pb_2Fe_2Ge_2O_9$ the germanate analogue of the silicate mineral melanotekite. Acta Crystallographica, C54, 2–5.

Burns, P.C., Cooper, M.A., and Hawthorne, F.C. (1994) Jahn-Teller-distorted $Mn^{3+}O_6$ octahedra in fredrikssonite, the fourth polymorph of $Mg_2Mn^{3+}(BO_3)O_2$. The Canadian Mineralogist, 32, 397–403.

Chen, S., Zhao, B., Hayes, P.C., and Jak, E. (2001) Experimental study of phase equilibria in the PbO-Al_2O_3-SiO_2 system. Metallurgical and materials transactions, B32, 997–1005.

Downs, R.T., Hazen, R.M., and Finger, L.W. (1995) Crystal chemistry of lead aluminosilicate hollandite: A new high-pressure synthetic phase with octahedral Si. American Mineralogist, 80, 937–940.

Gabelica-Robert, M. and Tarte, P (1979) Synthesis, X-ray diffraction and vibrational study of silicates and germanates isostructural with kentrolite $Pb_2Mn_2Si_2O_9$. Journal of Solid State Chemistry, 27, 179–190.

Gabrielson, O. (1961) The crystal structures of kentrolite and melanotekite. Arkiv för Mineralogy och Geologie, 3(7), 141–151.

Glasser, F.P. (1967) New data on kentrolite and melanotekite: Ternary phase relations in the system PbO-Fe_2O_3-SiO_2. American Mineralogist, 52, 1085–1093.

Ito, J. (1968) Synthetic indium silicate and indium hydrogarnet. American Mineralogist, 53, 1663–1673.

Ito, J. and Frondel, C. (1966) Syntheses of the kentrolite-melanotekite series. Arkiv för Mineralogy och Geologie, 4(14), 387–390.

——— (1968) Syntheses of the scandium analogues of aegirine, spodumene, andradite, and melanotekite. American Mineralogist, 53, 1276–1280.

Krivovichev, S.V. and Burns, P.C. (2001) Crystal chemistry of lead oxide chlorides. I. Crystal structures of synthetic mendipite, $Pb_3O_2Cl_2$, and synthetic damaraite, $Pb_3O_2(OH)Cl$. European Journal of Mineralogy, 13, 801–809.

——— (2002) Crystal chemistry of lead oxide chlorides. II. Crystal structure of $Pb_7O_4(OH)_4Cl_2$. European Journal of Mineralogy, 14, 135–139.

Moore, P.B. and Araki, T. (1979) Crystal structure of synthetic $Ca_3Mn^{3+}_2O_2(Si_4O_{12})$, Zeitschrift für Kristallographie, 150, 287–297.

Moore, P.B., Sen Gupta, P.K., Shen, J., and Schlemper, E.O. (1991) The kentrolite-melanotekite series, $4Pb_2(Mn,Fe)^{3+}_2O_2(Si_2O_7)$: Chemical crystallographic relations, lone-pair splitting, and cation relation to $8URe_2$. American Mineralogist, 76, 1389–1399.

Morita, S. and Toda, K. (1984) Determination of the crystal structure of Pb_2CrO_5. Journal of Applied Physics, 55(7), 2733–2737.

Pouchou, J.L. and Pichoir, F. (1984) Un nouveau modèle de calcul pour la microanalyse quantitative par spectrométrie de rayons X. La Recherche Aérospatiale, 3, 167–192.

Shannon, R.D. (1976) Revised effective ionic radii and systematic studies of interatomic distances in halides and chalcogenides. Acta Crystallographica, A32, 751–767.

Shannon, R.D., Gumerman, P.S., and Chenavas, J. (1975) Effect of octahedral distortion on mean Mn^{3+}-O distances. American Mineralogist, 60, 714–716.

Sheldrick, G.M. (1993) SHELXL-93. Program for the refinement of crystal structures, University of Göttingen, Germany.

Spek, A.L. (2005) PLATON, A multipurpose crystallographic tool. Utrecht University, The Netherlands.

Tribaudino, M., Benna, P., and Bruno, E. (1998) Structural variations induced by thermal treatment in lead feldspar ($PbAl_2Si_2O_8$). American Mineralogist, 83, 159–166.

Werner, J.-P. and Müller-Buschbaum, H. (1997) Zur Kenntnis eines synthetischen Kentrolits/Melanotekits des Indiums: $Pb_2In_2Si_2O_9$. Zeitschrift für Naturforschung, B 52, 1213–121.

Wunder, B. and Melzer, S. (2002) Interlayer vacancy characterization of synthetic phlogopitic micas by IR spectroscopy. European Journal of Mineralogy, 14, 1129–1138.

MANUSCRIPT RECEIVED FEBRUARY 4, 2007
MANUSCRIPT ACCEPTED NOVEMBER 12, 2007
MANUSCRIPT HANDLED BY SERGEY KRIVOVICHEV